

Towards Event-Triggered NMPC for Efficient 6G Communications: Experimental Results and Open Problems

Jens Püttschneider, Julian Golembiewski, Niklas A. Wagner, Christian Wietfeld, Timm Faulwasser

Abstract—Networked control systems enable real-time control and coordination of distributed systems, leveraging the low latency, high reliability, and massive connectivity offered by 5G and future 6G networks. Applications include autonomous vehicles, robotics, industrial automation, and smart grids. Despite networked control algorithms admitting nominal stability guarantees even in the presence of delays and packet dropouts, their practical performance still heavily depends on the specific characteristics and conditions of the underlying network. To achieve the desired performance while efficiently using communication resources, co-design of control *and* communication is pivotal. Although periodic schemes, where communication instances are fixed, can provide reliable control performance, unnecessary transmissions, when updates are not needed, result in inefficient usage of network resources. In this paper, we investigate the potential for co-design of model predictive control and network communication. To this end, we design and implement an event-triggered nonlinear model predictive controller for stabilizing a Furuta pendulum communicating over a tailored open radio access network 6G research platform. We analyze the control performance as well as network utilization under varying channel conditions and event-triggering criteria. Our results show that the event-triggered control scheme achieves similar performance to periodic control with reduced communication demand.

I. INTRODUCTION

Networked Control Systems (NCS), enabling distributed wirelessly connected plant and controller architectures, are one major use case enabled by 5G and future 6G networks [1]. However, despite the advances in network development, delays, packet loss, limited bandwidth, energy consumption, and reliability remain a challenge for NCS and need to be addressed by co-design of control and communication [2]. Co-design strategies include delay compensation [3], acknowledgments for handling packet losses [4], energy-efficient communication policies [5], and event-based control [6].

Event-based control reduces the communication demand while maintaining the control performance [6] and thus

This work has been partly funded by the Federal Ministry of Education and Research (BMBF) via the project *6GEM* under funding reference 16KISK038, the Deutsche Forschungsgemeinschaft (DFG, German Research Foundation) under project number 508759126, and by the Ministry for Economic Affairs, Industry, Climate Action and Energy (MWIKE) of the State of North Rhine-Westphalia via the project *Shine* under funding reference 005-2108-0074.

Jens Püttschneider, **Julian Golembiewski**, Institute of Energy Systems, Energy Efficiency and Energy Economics, TU Dortmund University, Dortmund, Germany {jens.puettschneider, julian.golembiewski}@tu-dortmund.de

Niklas A. Wagner, **Christian Wietfeld**, Communication Networks Institute (CNI), TU Dortmund University, Dortmund, Germany {niklas.wagner, christian.wietfeld}@tu-dortmund.de

***Timm Faulwasser**, Institute of Control Systems, Hamburg University of Technology, Hamburg, Germany timm.faulwasser@ieee.org

enables networked control with limited network bandwidth. For an overview of event-based control we refer to [6], [7]. Event-based control encompasses two primary approaches: event-triggered control and self-triggered control. In event-triggered control, an input is applied in sample-and-hold fashion until a predefined triggering condition is met, typically when the state deviates significantly from a predicted value [8]. In self-triggered control, on the other hand, the recalculation time is determined by the controller and calculated at the same time as the control input [9]. Event-based control is especially powerful in combination with Model Predictive Control (MPC), which computes its feedback by optimizing an open-loop trajectory that can be applied until a triggering criterion, based on the deviation of the state to the predicted trajectory is met [10].

Despite this extensive theoretical analysis of event-triggered MPC and event-triggered control more broadly, most papers illustrate the proposed schemes via numerical simulations only [10]–[13]. As highlighted in [12], experimental studies are crucial for advancing research in NCS. They provide valuable insights into control performance and communication resource requirements for control applications in both current and future wireless networks. Only a limited number of works explore real hardware implementations: [14], [15] implement their applications using wired experimental setups. Likewise, [16] evaluates event-based control in a real-world scenario with idealized communication assumptions. A hardware-in-the-loop distributed model predictive control experiment is presented in [17], using a simulated wireless network. In [18], an event-triggered scheme for a nonlinear system is implemented and its performance is compared to that of a periodic controller. Plant and controller communicate over the contention-based low-power IEEE 802.15.4 wireless network. In our previous work [19] we evaluated the impact of different resource scheduling strategies on delay and control performance of a delay-compensated periodic Nonlinear Model Predictive Control (NMPC) implementation.

Extending our previous work, this paper investigates the potential of event-triggered control via 5G and future 6G networks. To the best of our knowledge, this work is the first to implement event-triggered NMPC within a 5G network. We experimentally validate the controller and analyze the trade-off between control performance and network load considering varying triggering criteria and channel conditions in a state-of-the-art network environment. Specifically, we use a 5G Open Radio Access Network (O-RAN), which provides enhanced reliability under high network loads compared to

contention-based IEEE 802.11 (Wi-Fi) [20] and serves as a research platform towards future 6G communication.

The remainder of this paper is structured as follows: Section 2 formally defines the problem and outlines the design of the proposed controller, including a stability analysis. Section 3 provides details of the experimental setup, implementation, and results, along with a discussion of the findings. Finally, Section 4 concludes the paper and discusses potential directions for future work.

II. PROBLEM STATEMENT & CONTROLLER DESIGN

We consider the task of controlling a nonlinear plant by an event-triggered controller connected by a communication network. Consider the continuous time nonlinear system

$$\dot{x}(t) = f(x(t), u(t)), \quad x(0) = x_0, \quad (1)$$

with state constraints $x(t) \in \mathbb{X} \subseteq \mathbb{R}^n$ and admissible inputs $u(t) \in \mathbb{U} \subseteq \mathbb{R}^m$ for all $t \in \mathbb{R}$. In this work, we assume full state feedback is available.

The plant is connected to the networked controller as shown in Figure 1. At sampling time t_k , the sensor measures the state of the plant $x(t_k)$. Based on the latest input trajectory and the corresponding state measurement, the sensor calculates the predicted state $\hat{x}(t_k)$. If the deviation of predicted state and current measurement exceeds the event-triggering threshold ε , i.e., if $\|x(t_k) - \hat{x}(t_k)\| \geq \varepsilon$, the sensor sends the current measurement and its timestamp to the controller.

The controller receives the message with the varying uplink delay $\tau_{UL}(t_k)$. Then, calculating the control law takes τ_C , and finally the control trajectory is communicated back to the actor and applied to the plant, which introduces a delay of τ_{DL} . The downlink and controller delays are assumed to be constant, thus the overall round-trip time

$$\tau_{RTT}(t_k) = \tau_{UL}(t_k) + \tau_C + \tau_{DL}$$

can be calculated by the controller based on the timestamp of the received state, assuming time synchronization between plant and controller.

Then, the controller compensates the delay by predicting the state

$$\hat{x}(t_k + \tau_{RTT}(t_k)) = x(t_k) + \int_{t_k}^{t_k + \tau_{RTT}(t_k)} f(x(t), u(t)) dt. \quad (2)$$

The input trajectory required for the delay compensation is stored in a buffer at the controller. The key challenge in designing a network controller with stability guarantees is the input consistency: The input trajectory used for the delay compensation has to match the one applied to the plant in the closed loop in spite of delays and packet losses [3], [10].

A. Proposed Control Scheme

The networked control Algorithm 1 is an adaptation of [10, Algorithm 1] for a deterministic downlink and controller

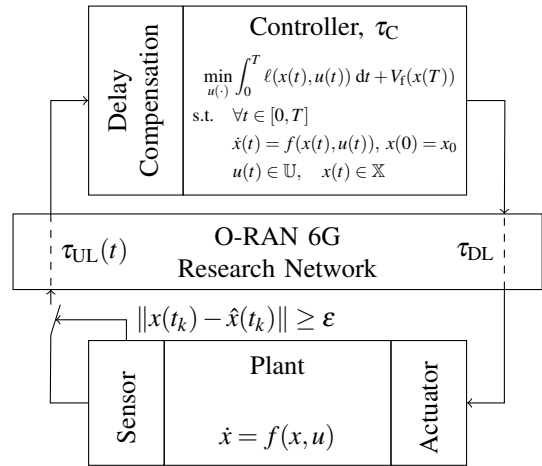


Fig. 1: Networked Control System.

delay. The controller solves the continuous time Optimal Control Problem (OCP)

$$\min_{u(\cdot)} \int_0^T \ell(x(t), u(t)) dt + V_f(x(T)) \quad (3a)$$

$$\text{s.t. } \forall t \in [0, T] \quad (3b)$$

$$\dot{x}(t) = f(x(t), u(t)), \quad x(0) = x_0 \quad (3c)$$

$$u(t) \in \mathbb{U} \quad (3d)$$

$$x(t) \in \mathbb{X} \quad (3e)$$

$$x(T) \in \mathbb{X}_f. \quad (3f)$$

The controller then sends the first part of the optimal input trajectory $u^*(t)$ for all $t \in [0, T_{\text{com}}]$, where T_{com} is the communicated horizon.

To initialize the delay compensation, the control input applied to the system before the first package is received needs to be known, which can be practically achieved, e.g., by starting with a zero input on both controller and actuator side.

B. Stability Analysis

We now turn towards the nominal stability guarantees of the proposed scheme. The next result can be found in [10].

Theorem 1 (Stability [10, Theorem 4.1]): Consider Algorithm 1 using OCP (3) with terminal penalty $V_f(x)$ and terminal region \mathbb{X}_f such that

- i) $V_f \in C^1$, $V_f(0) = 0$, and $\mathbb{X}_f \subset X$ is closed, connected and contains the origin
- ii) There exist T such that $0 < \delta \leq t_{i+1} - t_i < T$, for all $i \in \mathbb{N}$ and some $\delta \in \mathbb{R}^+$
- iii) For all $x_0 \in \mathbb{X}_f$, there exists $u(\tau) \in U$, $\tau \in [0, T]$ such that

$$x(\tau) \in \mathbb{X}_f, \quad (4a)$$

$$\dot{x}(\tau) = f(x(\tau), u(\tau)), \quad x(0) = x_0, \quad (4b)$$

$$\frac{\partial V_f}{\partial x} f(x(\tau), u(\tau)) + \ell(x(\tau), u(\tau)) \leq 0 \quad (4c)$$

- iv) OCP (3) is feasible at t_0 .

Then $\lim_{t \rightarrow \infty} \|x(t)\| \rightarrow 0$.

Algorithm 1 Networked Control System Algorithm

Sensor

- 1: **for** each sampling time t_k **do**
- 2: Measure state $x(t_k)$
- 3: Compute $\hat{x}(t_k)$ based on the latest input trajectory $(u(\cdot), t_x)$ and the corresponding state measurement $x(t_x)$
- 4: **if** $\|x(t_k) - \hat{x}(t_k)\| \geq \varepsilon$ **then**
- 5: Send the packet $(x(t_k), t_k)$ to the controller
- 6: Save the current state measurement (x_k, t_k)
- 7: **end if**
- 8: **end for**

Controller

- 1: `control_input_buffer` = $\{(u^*(\cdot), t_0 + \tau_{RTT}(t_0))\}$
- 2: $t_{old} = t_0$
- 3: **while** True **do**
- 4: Wait for the package $(x(t_k), t_k)$
- 5: **if** $t_k > t_{old}$ **then**
- 6: $t_{old} = t_k$
- 7: Calculate the round-trip time $\tau_{RTT}(t_k) = t - t_k + \tau_C + \tau_{DL}$
- 8: Apply the delay compensation (2) to obtain $\hat{x}(t_k + \tau_{RTT}(t_k))$
- 9: Solve OCP (3) with $x_0 = \hat{x}(t_k + \tau_{RTT}(t_k))$
- 10: Send the first part of the optimal input trajectory and the state timestamp to the actuator as $u^*(t), t \in [t_k + \tau_{RTT}(t_k), t_k + \tau_{RTT}(t_k) + T_{com}]$ ($u(\cdot), t_k + \tau_{RTT}(t_k)$)
- 11: Append $(u(\cdot), t_k + \tau_{RTT}(t_k))$ to the `control_input_buffer`
- 12: **end if**
- 13: **end while**

Actuator

- 1: **while** True **do**
 - 2: Receive the input trajectory packet $(u(\cdot), t_x)$ at time $t_k + \tau_{RTT}(t_k)$
 - 3: Start applying the newly received control input $u(\cdot)$
 - 4: Provide the input trajectory to the sensor $(u(\cdot), t_x)$
 - 5: **end while**
-

We now extend the previous analysis to derive stability without terminal region.

Theorem 2 (Stability without Terminal Region):

Consider Algorithm 1 using OCP (3) such that stability is guaranteed by Theorem 1 for the terminal region $\mathbb{X}_f = \{x \in \mathbb{X} \mid V_f(x) \leq \gamma\}$ with $\gamma > 0$. Then, for any initial condition from which $x = 0$ can be reached in finite time, there exists $\beta < \infty$, such that the OCP without terminal constraint $\mathbb{X}_f = \mathbb{X}$ and weighted terminal penalty $V_{f,\beta}(x) = \beta V_f(x)$ guarantees asymptotic convergence, i.e. $\lim_{t \rightarrow \infty} \|x(t)\| \rightarrow 0$.

Proof: Due to space limitations we only give a brief sketch of the proof. The NMPC scheme considered is an adaptation of Algorithm 1. A straight-forward continuous-time extension of [21, Theorem 3] shows convergence with-

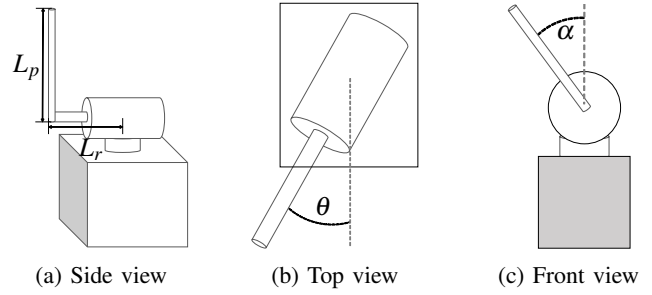


Fig. 2: Furuta pendulum schematic with length L_r and angle θ for the rotary arm as well as length L_p and angle α for the pendulum arm.

out delays, whereby, if β is chosen sufficiently large, the terminal constraint (3f) is satisfied without being explicitly considered. Closed-loop convergence follows by Theorem 1. \blacksquare

III. EXPERIMENTS

Next, we discuss the experiments for the proposed event-triggered NMPC controller. We begin by presenting the experimental setup, which comprises a rotational inverted pendulum and a tailored O-RAN research system for 6G. This is followed by a detailed analysis of the experimental results.

A. System Model and OCP Design

The control plant used in our experiments is a rotational inverted pendulum, specifically a Furuta pendulum [22], the Quanser Servo 2. This system consists of a motor-driven rotary arm to which a pendulum link is attached, see Figure 2. The state vector $x = (\theta, \alpha, \dot{\theta}, \dot{\alpha})^T \in \mathbb{R}^4$ comprises the rotary arm angle $\theta \in [-\pi/2, \pi/2]$, the pendulum arm angle α , and their respective angular velocities $\dot{\theta}$ and $\dot{\alpha}$. The link lengths are denoted by L_p and L_r . The control input $u \in [-7.5, 7.5]$ is the voltage applied to the motor that drives the rotary arm.

The Furuta pendulum dynamics $\dot{x} = f(x, u)$ are derived similar to [22] and the resulting nonlinear equations of motion read

$$\left(m_p L_r^2 + \frac{1}{4} m_p L_p^2 s^2(\alpha) + J_r \right) \ddot{\theta} - \frac{1}{2} m_p L_p L_r c(\alpha) \ddot{\alpha} + \frac{1}{2} m_p L_p L_r s(\alpha) \dot{\alpha}^2 + \frac{1}{2} m_p L_p^2 s(\alpha) c(\alpha) \dot{\alpha} \dot{\theta} = \tau - B_r \dot{\theta}, \quad (5a)$$

$$-\frac{1}{2} m_p L_p L_r c(\alpha) \ddot{\theta} + \left(J_p + \frac{1}{4} m_p L_p^2 \right) \ddot{\alpha} - \frac{1}{4} m_p L_p^2 c(\alpha) s(\alpha) \dot{\theta}^2 - \frac{1}{2} m_p L_p g s(\alpha) = -B_p \dot{\alpha}, \quad (5b)$$

$$\tau = \frac{k_t (u - k_m \cdot \dot{\theta})}{R_m}. \quad (5c)$$

We use $s(\cdot)$ and $c(\cdot)$ to denote the sine and cosine function respectively. The parameters and their values are given in Table I.

TABLE I: Parameters of the Furuta Pendulum.

Parameter	Value	Description
R_m	8.4Ω	Resistance
k_t	$0.042 \text{ N}\cdot\text{m/A}$	Current-torque constant
k_m	$0.042 \text{ V}\cdot\text{s/rad}$	Velocity constant
m_r	0.095 kg	Mass of rotary arm
L_r	0.085 m	Total length of rotary arm
J_r	$5.72 \times 10^{-5} \text{ kg}\cdot\text{m}^2$	Moment of inertia of rotary arm
D_r	$2.7 \times 10^{-4} \text{ m}\cdot\text{s/rad}$	Viscous damping of rotary arm
m_p	0.024 kg	Mass of pendulum link
L_p	0.129 m	Total length of pendulum link
J_p	$3.33 \times 10^{-5} \text{ kg}\cdot\text{m}^2$	Moment of inertia of pendulum link
D_p	$5 \times 10^{-5} \text{ N}\cdot\text{m}\cdot\text{s/rad}$	Viscous damping of pendulum link
g	9.81 m/s^2	Gravitational acceleration

We design OCP (3) to stabilize the system at its upper equilibrium $x_{\text{goal}} = (0, 0, 0, 0)^\top$, starting from its lower equilibrium $x_0 = (0, -\pi, 0, 0)^\top$. This requires a swing-up from the initial position. The stage cost and terminal penalty are defined as $\ell(x(t), u(t)) = 1/2 x(t)^\top Q x(t) + 1/2 R u(t)^\top u(t)$ and $V_f(x) = 1/2 x^\top P x$, respectively, where $Q = \text{diag}(1.6, 1.6, 0.1, 0.01)$, $R = 0.4$, and P is the solution of the algebraic Riccati equation for the linearized dynamics at the upper equilibrium. We observe stability for $\beta = 1$, since the prediction horizon is long enough to swing the pendulum up. State and input constraints are imposed based on the physical limitations of the system, maximum motor torque and rotary arm angle. The state constraints on the rotary arm angle are implemented as soft constraints. The slacks $s_{\text{ub}}, s_{\text{lb}} : [0, T] \rightarrow \mathbb{R}^+$ for the upper bound $\theta(t) - \pi/2 \leq s_{\text{ub}}(t)$ and lower bound $s_{\text{lb}}(t) \geq \theta(t) + \pi/2$ are penalized within the stage cost by $\ell_s(x) = 0.1 \cdot (s_{\text{lb}}^2 + s_{\text{ub}}^2) + s_{\text{lb}} + s_{\text{ub}}$. For real-time computation, the resulting OCP is implemented in the Acados framework [23]. We use a prediction horizon of $T = 2 \text{ s}$ with $N = 50$ stages and a variable sampling time. The ten initial stages, which are more likely to be applied in the event-triggered NMPC loop, are discretized with a finer sampling interval of $\Delta t = 20 \text{ ms}$, while the remaining trajectory uses a coarser discretization with $\Delta t = 45 \text{ ms}$. The length of the communicated trajectories $T_{\text{com}} = 200 \text{ ms}$ is designed to match the finer discretization of the ten initial stages. Finally, we use the closed-loop cost J_{CL} as a metric to evaluate control performance over the experiment duration T_{CL} in our experiments:

$$J_{\text{CL}} = \frac{1}{T_{\text{CL}}} \int_0^{T_{\text{CL}}} \ell(x(t), u(t)) dt. \quad (6)$$

B. Communication Setup

For the real-world O-RAN communication testbed, we employ an open 5G stack as a basis, allowing for flexible adaptation of cell parameters to the specific needs of control systems including low latency and reduced jitter, i.e., variance of latency [19]. The use of cellular networks like 5G over contention-based networks, such as the commonly used Wi-Fi, is persistent reliability, also under high network load [20]. The 5G system is realized using the O-RAN stack *srsRAN Project* [24], the core network Open5GS, and an NI USRP X310 Software-Defined Radio (SDR). We employ

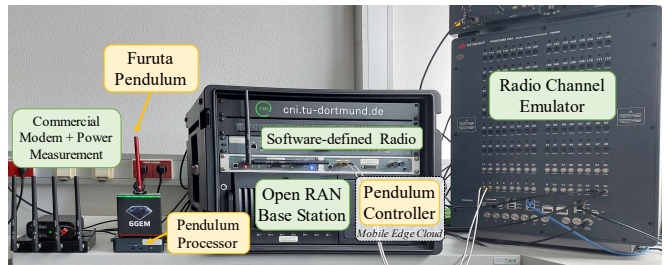


Fig. 3: Experimental setup comprising the Furuta pendulum and the O-RAN 6G communication research platform.

a commercial-grade Quectel RM520Q-GL 5G modem to provide connectivity for the pendulum. To lower average latency and jitter, we tune the reactive uplink scheduling strategy so that the modem can request uplink resources at the radio resource scheduling of the base station every 4 ms. The adaption comes at the cost of higher total radio resources due to overhead by the high scheduling frequency. To reduce latency induced by waiting times, we set tight timing requirements on the modem. This includes the time between uplink resource grant and uplink data transmission, as well as the delay for downlink data acknowledgments. On the transport layer, we use the user datagram protocol.

To challenge the control algorithm with realistic channel conditions, we employ a Prosim F64 real-time radio channel emulator realizing a Tapped-Delay-Line C fading channel with a delay spread of 300 and maximum doppler frequency of 100 Hz as defined by 3GPP standardization in [25]. Additionally, we challenge the algorithm with different Signal-to-Noise-Ratios (SNRs) to force packet errors of up to 80 %, resulting in either higher latency in case of packet re-transmission by the Hybrid-Automatic-Repeat Request (HARQ) mechanism of 5G or result in packet loss if undetected. Hence, we can provide realistic scenarios including far cell-edge deployments of the control application. For reproducible conditions, we setup an SNR with variable interference power distributed as Additive White Gaussian Noise (AWGN) to force a given SNR, resulting in bit errors. Hence, the modulation and coding is successively reduced by the channel adaptation mechanisms to reduce packet failures up to the most robust possible coding, after which errors inevitably appear. Before, the rapidly changing channel defined by the channel model leads to minor errors.

C. Experimental Results

We analyze the trade-off between closed-loop cost (6) and the communication demand relative to periodic control for varying event-triggering thresholds ϵ . We also investigate the impact of the varying channel conditions on the delay pattern and the resulting control performance. The results are shown in Figure 4 and 5, respectively. Each bar shows the average value for a total of five measurements, where each run consists of swinging up and stabilizing the Furuta pendulum for an experiment duration of $T_{\text{CL}} = 30 \text{ s}$.

First, the pendulum is controlled over the air interface

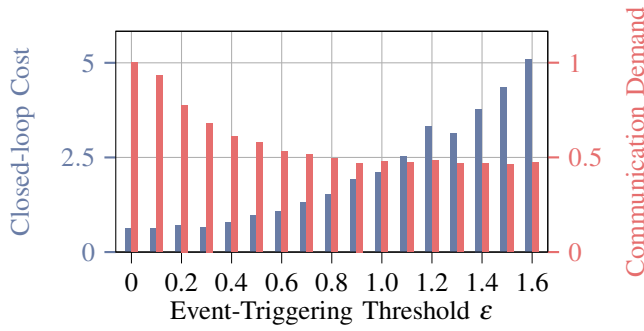


Fig. 4: Closed-loop cost and communication demand over the event-triggering threshold ϵ .

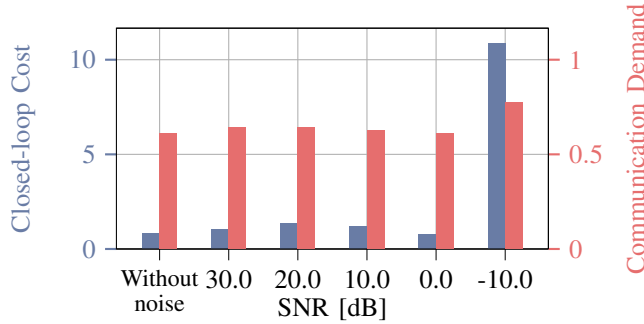


Fig. 5: Closed-loop cost and communication demand over varying channel signal-to-noise ratio.

using antennas without modifying the channel conditions for varying event-triggering thresholds ϵ . A threshold of $\epsilon = 0$ corresponds to periodic control and therefore a communication demand of 100%. With increasing ϵ , the recalculation of the closed-loop solution becomes less frequent, and the open-loop control input is applied for a longer duration, resulting in a higher closed-loop cost, as illustrated in Figure 4. On the other hand, this reduces the frequency of control signal transmissions over the wireless interface, thereby lowering the communication demand. Dependent on the application requirements, we observe the best trade-off between control performance and communication demand. For the Furuta pendulum, we consider $\epsilon = 0.4$ as a suitable threshold. In this case, the communication demand is reduced to 61% network traffic with a negligible impact on the control performance. Next, we keep $\epsilon = 0.4$ constant while using the radio channel emulator to provide a challenging channel and force packet errors via a decreasing SNR towards far cell-edge. The results are shown in Figure 5. The closed-loop cost and communication demand are comparable for SNR values above 0dB. However, at -10 dB, increased channel noise leads to significant packet dropouts and higher latencies, preventing the controller from stabilizing the system. This is reflected in the increased closed-loop cost. To understand the factors influencing the controller performance, we analyze the delays at an SNR of -10 dB. Figure 6 shows the results for a single experiment run, depicting the RTT and the state α , which represents the angle of the pendulum arm. The

setpoint $\alpha = 0$ is indicated by a dashed green line. The results show that the plant remains stable even with latency peaks exceeding 100 ms. However, when multiple correlated latency peaks occur around the $t = 18$ s mark, the controller fails to maintain stability, causing the pendulum arm to fall and leading to an increased closed-loop cost.

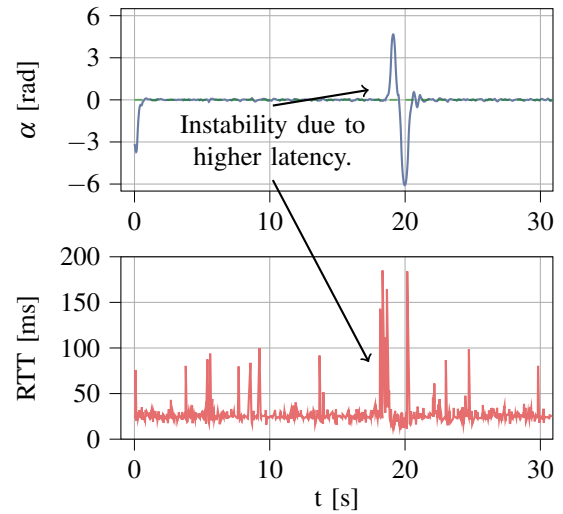


Fig. 6: Pendulum arm α and RTT for SNR = -10 dB.

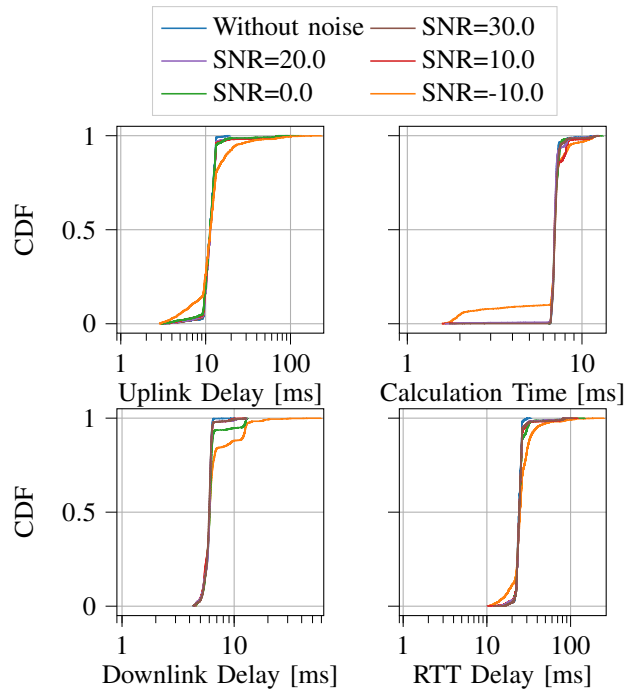


Fig. 7: Delay components for different SNR values.

setpoint $\alpha = 0$ is indicated by a dashed green line. The results show that the plant remains stable even with latency peaks exceeding 100 ms. However, when multiple correlated latency peaks occur around the $t = 18$ s mark, the controller fails to maintain stability, causing the pendulum arm to fall and leading to an increased closed-loop cost.

To analyze the delay distribution in more detail, we show the cumulative distribution function (CDF) of the delays for varying SNR values in Figure 7 and the corresponding average delays in Table II. For the settings without added noise and good SNR values of 30, 20, and 10 dB, the delays are

TABLE II: Average of the delays for different SNR values.

SNR [dB]	Uplink Delay [ms]	Calculation Time [ms]	Downlink Delay [ms]	RTT Delay [ms]
Baseline	11.22	7.04	5.90	24.16
30.0	12.06	7.09	5.95	25.10
20.0	11.91	7.03	5.98	24.92
10.0	12.11	7.13	5.94	25.17
0.0	11.76	7.07	6.30	25.13
-10.0	13.45	6.80	6.99	27.20

centered closely around their average values since no to little significant transmission errors occur. In the uplink direction under low signal level, resulting in an SNR of -10 dB, a large part of the available resources are allocated to the critical pendulum UE. Here, uplink resource over-allocations happen and the UE can send data without sending scheduling requests, resulting in lower-latency outliers. These outliers below and above the average delay are at around 6 ms. However, if multiple re-transmissions are needed to transmit a packet without errors, uplink delays of up to 180 ms are observed. The problems with instability for the case of -10 dB also lead to an early termination of the OCP calculation and thus reduced calculation times. Meanwhile, the downlink transmission errors occurring for SNR values of 0 dB and -10 dB lead to HARQ re-transmissions and a second accumulation of downlink delays at around 12 ms, twice the delay without transmission errors.

IV. CONCLUSIONS & OUTLOOK

This paper illustrates the potential of co-design of networked control via future 6G networks by providing first experimental results of event-triggered NMPC within a 6G research platform. Even for the challenging task of stabilizing an inverted pendulum in its upper equilibrium, event-triggered control reduces communication demand to 61 % compared to periodic control while maintaining similar control performance. While the networked control system is robust to delays up to 100 ms, prolonged delays due to poor channel conditions can affect the stability of the control application. Future work will examine how event-triggered control impacts energy consumption and battery life in networked control systems. Additionally, further experiments with diverse control applications and communication systems are needed to advance networked control applications.

REFERENCES

[1] M. Giordani, M. Polese, M. Mezzavilla, S. Rangan, and M. Zorzi, "Toward 6G networks: Use cases and technologies," *IEEE Communications Magazine*, vol. 58, no. 3, pp. 55–61, 2020.

[2] G. Zhao, M. A. Imran, Z. Pang, Z. Chen, and L. Li, "Toward real-time control in future wireless networks: Communication-control co-design," *IEEE Communications Magazine*, vol. 57, no. 2, pp. 138–144, 2019.

[3] P. Varutti, "Model predictive control for nonlinear networked control systems," Ph.D. dissertation, Shaker GmbH Aachen, 2014.

[4] V. Dolk and W. Heemels, "Dynamic event-triggered control under packet losses: The case with acknowledgements," in *2015 International Conference on Event-based Control, Communication, and Signal Processing (EBCCSP)*, IEEE, 2015, pp. 1–7.

[5] V. S. Varma, A. M. de Oliveira, R. Postoyan, I.-C. Morărescu, and J. Daafouz, "Energy-efficient time-triggered communication policies for wireless networked control systems," *IEEE Transactions on Automatic Control*, vol. 65, no. 10, pp. 4324–4331, 2020.

[6] W. Heemels, K. Johansson, and P. Tabuada, "An introduction to event-triggered and self-triggered control," in *2012 IEEE 51st IEEE Conference on Decision and Control (CDC)*, 2012, pp. 3270–3285.

[7] C. Peng and F. Li, "A survey on recent advances in event-triggered communication and control," *Information Sciences*, vol. 457, pp. 113–125, 2018.

[8] K.-E. Årzén, "A simple event-based PID controller," *IFAC Proceedings Volumes*, vol. 32, no. 2, pp. 8687–8692, 1999.

[9] P. Marti, J. M. Fuertes, G. Fohler, and K. Ramamritham, "Improving quality-of-control using flexible timing constraints: Metric and scheduling," in *23rd IEEE Real-Time Systems Symposium, 2002. RTSS 2002.*, IEEE, 2002, pp. 91–100.

[10] P. Varutti, B. Kern, T. Faulwasser, and R. Findeisen, "Event-based model predictive control for networked control systems," in *Proceedings of the 48th IEEE Conference on Decision and Control (CDC) held jointly with 2009 28th Chinese Control Conference*, IEEE, 2009, pp. 567–572.

[11] Q. Wang, Y. Zou, and Y. Niu, "Event-triggered model predictive control for wireless networked control systems with packet losses," in *2015 IEEE International Conference on Cyber Technology in Automation, Control, and Intelligent Systems (CYBER)*, 2015, pp. 1281–1286.

[12] M. Balaghiinaloo, "Consistent event-triggered control for linear systems," Ph.D. dissertation, Eindhoven University of Technology, 2020.

[13] H. Yang, X. Guo, L. Dai, and Y. Xia, "Event-triggered predictive control for networked control systems with network-induced delays and packet dropouts," *International Journal of Robust and Nonlinear Control*, vol. 28, no. 4, pp. 1350–1365, 2018.

[14] Z. Zhou, J. Chen, M. Tao, P. Zhang, and M. Xu, "Experimental validation of event-triggered model predictive control for autonomous vehicle path tracking," in *2023 IEEE International Conference on Electro Information Technology (eIT)*, 2023, pp. 35–40.

[15] B. Wang, J. Huang, C. Wen, J. Rodriguez, C. Garcia, H. B. Gooi, and Z. Zeng, "Event-triggered model predictive control for power converters," *IEEE Transactions on Industrial Electronics*, vol. 68, no. 1, pp. 715–720, 2021.

[16] D. Lehmann and J. Lunze, "Extension and experimental evaluation of an event-based state-feedback approach," *Control Engineering Practice*, vol. 19, no. 2, pp. 101–112, 2011.

[17] A. Gräfe, J. Eickhoff, and S. Trimpe, "Event-triggered and distributed model predictive control for guaranteed collision avoidance in uav swarms," *IFAC-PapersOnLine*, vol. 55, no. 13, pp. 79–84, 2022.

[18] F. Altaf, J. Araújo, A. Hernandez, H. Sandberg, and K. H. Johansson, "Wireless event-triggered controller for a 3D tower crane lab process," in *2011 19th Mediterranean Conference on Control & Automation (MED)*, 2011, pp. 994–1001.

[19] D. Overbeck, N. A. Wagner, R. Wiebusch, J. Püttschneider, T. Faulwasser, and C. Wietfeld, "Data-driven proactive uplink slicing enabling real-time control within an open ran testbed," in *IEEE INFOCOM Workshops (INFOCOM WKSHPS)*, 2024.

[20] C. Arendt, S. C. Fricke, S. Böcker, and C. Wietfeld, "Distributed performance evaluation of 5G and Wi-Fi for private industrial networks," in *IEEE International Symposium on Personal, Indoor, and Mobile Radio Communications (PIMRC)*, 2024.

[21] D. Limón, T. Alamo, F. Salas, and E. F. Camacho, "On the stability of constrained MPC without terminal constraint," *IEEE transactions on automatic control*, vol. 51, no. 5, pp. 832–836, 2006.

[22] K. Furuta, M. Yamakita, and S. Kobayashi, "Swing-up control of inverted pendulum using pseudo-state feedback," *Proceedings of the Institution of Mechanical Engineers, Part I: Journal of Systems and Control Engineering*, vol. 206, no. 4, pp. 263–269, 1992.

[23] R. Verschuere, G. Frison, D. Kouzoupis, J. Frey, N. van Duijkeren, A. Zanelli, B. Novoselnik, T. Albin, R. Quirynen, and M. Diehl, "Acados – a modular open-source framework for fast embedded optimal control," *Mathematical Programming Computation*, 2021.

[24] Software Radio Systems. "srsRAN Project: Open source O-RAN 5G CU/DU solution. v24.04." (2024), [Online]. Available: <https://docs.srsran.com/projects/project/en/latest/>.

[25] 3rd Gen. Partnership Project (3GPP), "Study on channel model for frequencies from 0.5 to 100 GHz," TR 38.901, 2024, v18.0.0.